Limit of monsoonal precipitation in southern Tibet during the Last Glacial Maximum from relative moraine extents

Marie-Luce Chevalier, Anne Replumaz, Shiguang Wang, Jiawei Pan, Mingkun Bai, Kaiyu Li, Haibing Li

Limit of monsoonal precipitation in southern Tibet during the Last Glacial Maximum from relative moraine extents

Geomorphology 397 (2022), doi:10.1016/j.geomorph.2021.108012

Marie-Luce Chevalier[*a,b], Anne Replumaz[c], Shiguang Wang[a,d], Jiawei Pan[a,b], Mingkun Bai[a,e], Kaiyu Li[a], Haibing Li[a,b]

a. Key Laboratory of Deep-Earth Dynamics of Ministry of Natural Resources, Institute of Geology, Chinese Academy of Geological Sciences, 26 Baiwanzhuang Rd, Beijing 100037, China

b. Southern Marine Science and Engineering Guangdong Laboratory (Guangzhou), Guangzhou 511458, China

c. ISTerre, Université Grenoble Alpes, CNRS, Grenoble, France

d. National Institute of Natural Hazards, Ministry of Emergency Management of China, Beijing, China

e. Peking University, Beijing, China

Keywords

Last Glacial Maximum; Yadong rift; moraine; Monsoon; Southern Tibet; Marine oxygen Isotope Stage; cosmogenic isotopes

Highlights

1. We dated one MIS-3 moraine at the base of >7000 m-high peaks in the Yadong rift
2. We dated one LGM moraine at the base of ~6000 m peaks with abundant LGM precipitation
3. We compiled ages from three N-S transects from northern Himalaya to central Tibet
4. LGM moraines > MIS-3 moraines only where LGM precipitation are strongest
5. We show new LGM monsoon limit from relative moraine extents

* Corresponding author: E-mail address: mlchevalier@hotmail.com, Tel.: +8613466654223

Abstract

Constraining the timing and extent of past glaciations can help understand how glaciers respond to climate change as well as study past changes in atmospheric circulation patterns, precipitation and temperature. Southern Tibet, thanks to its numerous, well-preserved, glacial deposits, is an ideal place to conduct such study, as it receives occasional winter precipitation from the mid-latitude Westerlies and abundant summer precipitation (snowfall at high elevation) from the Indian and East Asian monsoons. The fact that amounts of precipitation varied in space and time over the plateau, greatly influenced past glaciations, now recorded as successive moraine deposits. Here, we study two large moraines from the southern Yadong rift (China-Bhutan border) and determined (using 19 new ^{10}Be cosmogenic samples) that at Jichu, which is located at the base of high summits (~7000 m), glacial deposits were abandoned during Marine oxygen Isotope Stage (MIS)-3 (~29-57 ka), and that at Qudui, located at the base of lower summits (~6000 m), the moraine was deposited during the Last Glacial Maximum (LGM, 19-26.5 ka). Both moraines directly rest on top of presumably MIS-6 (~130-191 ka) remnant surfaces. We suggest that while abundant MIS-3 precipitation allowed MIS-3 moraines to be deposited at the base of the highest summits (such as at Jichu) despite warmer temperature than during the LGM, smaller amounts of precipitation occurred during colder MIS-2, blocked by high summits, preventing deposition of large LGM moraines. By contrast, where restricted LGM precipitation can easily reach across lower summits, large MIS-2 moraines exist at their base (such as at Qudui). In addition, we compiled published ages from 22 most extensive moraines (≤ MIS-6) from the northern Himalaya to central Tibet (211 samples) along three N-S transects (~50-400 km-long). We found that the relative extent of LGM and MIS-3 moraines varies between different regions, that we infer is due to spatial variations in precipitation: in general, MIS-3 (or maybe MIS-4 at places) moraines are more extensive than MIS-2 moraines, except in the Yadong rift, where LGM monsoon was able to reach, thanks to low topographic barrier and proximity to the monsoonal front. This thus allows to draw the limit of monsoonal precipitation during the LGM.

1. Introduction

The Tibetan Plateau being the most glaciated area outside of the polar regions is also called the third pole (e.g., Qiu, 2008; Yao et al., 2012). It is an ideal place to study past glaciations, in particular by studying imbricated moraines recording successive past glacial episodes, especially well-preserved on the flat plateau. Because past glaciations can record past changes in atmospheric circulation, precipitation and temperature, quantitatively constraining their extent and timing may help reconstruct past climate and improve our understanding on how glaciers respond to climate change. Indeed, mountain glaciers are highly sensitive to climate change, especially in zones influenced by various climatic systems such as the Tibetan Plateau. At present, the mid-latitude Westerlies bring winter precipitation mostly in northern and western Tibet, sometimes reaching southern Tibet (e.g., Mölg et al., 2013), and the Indian and East Asian monsoons bring summer precipitation mostly in southern and eastern Tibet (e.g., Benn and Owen, 1998; Herzschuh, 2006) (inset in Fig. 1). These climatic systems have varied through time (e.g., Zech et al., 2005; Wang et al., 2008) hence have greatly influenced glaciers fluctuation in Tibet, especially by controlling the amount of precipitation, hence the amount of snowfall at high elevation, received during both summer and winter, resulting in differences between monsoon-influenced regions and others. Due to its extensive size and high elevation, the Tibetan Plateau has influenced atmospheric circulation patterns, modified the path of the mid-latitude Westerlies, and modified the monsoon intensity (e.g., Ruddiman and Kutzbach, 1989; Prell and Kutzbach, 1992; Owen et al., 2005), so that past glaciations have also varied spatially (e.g., Benn and Owen, 1998).

Thanks to advances in dating techniques, an increasingly large number of glacial deposits, although far from exhaustive, has been dated across the Himalayan-Tibetan orogen, revealing the complex age pattern and apparent asynchronicity between different regions. Marine oxygen Isotope Stage (MIS)-6 deposits (~130-191 ka), which are among the oldest dated moraines, are observed both in semi-arid central Tibet such as in the Tanggula Mountains (Schäfer et al., 2002; Owen et al.,

2005) and in more humid eastern Tibet (e.g., Chevalier and Replumaz, 2019). However, many are often poorly-preserved compared to younger deposits hence are undated, making it difficult to assess their real spatial distribution. For MIS<6 moraines, Owen and Dortch (2014) suggested that glaciers in more humid regions (such as southern and eastern Tibet) reached their maximum extent during the global Last Glacial Maximum (gLGM, hereafter LGM, ~19-26.5 ka [Clark et al., 2009], during MIS-2, ~14-29 ka), later than those in semi- to arid regions (northern, western and central Tibet), where maximum extent occurred during MIS-3 (~29-57 ka) and LGM advances were limited. However, in humid eastern Tibet, sites with several imbricated moraines show that in spite of LGM moraines being the sharpest and best preserved deposits, MIS-6 moraines are the largest, although less sharp and relatively well-preserved at only a few places, while MIS-3 moraines are entirely missing from the glacial record (Chevalier and Replumaz, 2019). Note that occasional older, poorly-preserved moraines are sometimes observed thanks to particular tectonic settings (Chevalier et al., 2016; Chevalier and Replumaz, 2019). By contrast, in western Tibet, LGM moraines are limited in extent compared to MIS-3 moraines, hence suggesting that the maximum extent of glaciations in those regions occurred during MIS-3 (e.g., Gillespie and Molnar, 1995; Benn and Owen, 1998; Owen et al., 2002, 2010; Finkel et al., 2003; Hedrick et al., 2011). This has been interpreted as due to increased insolation during MIS-3, which drove monsoonal precipitation (snowfall) farther into the plateau, hence reaching western Tibet, resulting in a higher positive glacier mass balance despite higher temperatures during MIS-3 than during MIS-2 (e.g., Finkel et al., 2003). Therefore, the respective extent of LGM and MIS-3 glaciations appears to vary between different regions partly due to spatial variations in precipitation, so that glaciers in arid regions may be more sensitive to changes in precipitation (such as temporal migration of the monsoonal front) compared to glaciers in more humid regions, which may be more sensitive to changes in temperature (e.g., Zech et al., 2009; Dortch et al., 2013).

We choose the Yadong rift in southern Tibet, along which the Chomo Lhari Range forms a

natural border with Bhutan, located on the northern slopes of the Himalaya (Fig. 1A), to assess glaciers sensitivity to variations in precipitation and temperature. We dated two large moraines, Qudui and Jichu, which show contrasted results despite their close proximity and appearance, that we then compare with the handful of results from farther north along the Yadong-Gulu rift (Owen et al., 2005; Chevalier et al., 2011, 2020; Dong et al., 2014, 2017; Liu et al., 2017; Peng et al., 2019; Wang et al., 2020). To further compare the relative extent of MIS-2 and MIS-3 glacial advances with those elsewhere in southern Tibet, we also compile ages of the most extensive moraines from regional studies north of the Himalaya, along two additional ~N-S transects located west of the Yadong rift.

2. Regional setting

The ~500 km-long Yadong-Gulu rift is one of the seven main, ~N-S trending rifts that dissect the southern Tibetan Plateau, and it is one of the few that crosses the Himalaya. These rifts are bounded on one or two sides by active normal faults that open up large basins at the foot of high mountain ranges (e.g., Armijo et al., 1986) (Fig. 1A). The Yarlung Zangbo (or Brahmaputra) River separates the Yadong-Gulu rift into the northern Yadong-Gulu rift to the north and the Yadong rift to the south. To the north, the NE-trending Nyainqentanghula (NQTL) Range (summit at 7162 m) bounds the western side of the rift, while to the south, the Chomo Lhari Range (summit at 7315 m) acts as a natural border between China and Bhutan (Fig. 1A).

Chomo Lhari Range's western slopes (Tibet) are steep and narrow, <4 km from the crest to the base of the mountain, where the large (up to ~15 km wide) Pagri basin and Duoqing Co Lake lie (Fig. 1). The sharp limit/change of slope between the range and the flat basin is due to the active Yadong normal fault, which has vertically offset LGM moraines by ~20 m at rates of 0.9±0.3 mm/yr (corresponding to ~E-W extension rates of 0.8±0.3 mm/yr, Wang et al., 2020). By contrast, the eastern slopes of the range (Bhutan) are gently dipping for tens of km within deeply incised valleys

(Fig. 1A). Consequently, moraines to the west can broadly expand in all directions on the Pagri basin floor while the multiple moraines to the east are long and more confined into narrow valleys (e.g., Iwata et al., 2002). Present-day glaciers on the western slopes are only ~2 km-long and reach down to ~5000 m while on the eastern slopes, they are up to ~ 9 km-long and reach elevations of 4100 m. Along the Chomo Lhari Range and Pagri basin, glacial landforms such as cirques, U-shaped valleys, and moraines abound. In addition, at numerous places, hummocky surfaces with lobes of various shapes and sizes are present on top of the main moraine's northern, outer flanks, rarely over the southern flanks (Fig. 1).

Data from Duoqing Co Lake weather station shows modern mean annual precipitation of 388 mm and mean annual temperature of ~4°C (1960 to 2010) (Yang et al., 2013), on the same order as modern precipitation measurements in the nearby Karola pass (~550 mm), eastern NQTL Range (~400 mm) (Owen et al., 2005), or NW Bhutan (<500 mm, e.g., Bookhagen et al., 2006).

We study two moraine complexes from the southern Yadong rift, Qudui and Jichu, which originate from the western side of the Chomo Lhari Range, close to each other but in different topographic contexts: the Jichu moraine is located at the base of the highest summits (~7000 m), while the Qudui moraine is located at that of lower summits (~6000 m), with a series of even lower peaks (~5000-6000 m) in between the two sites, hence possibly influencing the amount of precipitation received from the monsoon (Fig. 1). Therefore, quantitatively constraining the timing and extent of past glaciations in the Yadong rift allows us to study how temperature and precipitation have influenced past Tibetan Himalayan glaciations. We further assess possible N-S and/or E-W differences, due to variations in precipitation, by comparing our results with similar studies farther north along the northern Yadong-Gulu rift, as well as farther west in neighboring rifts.

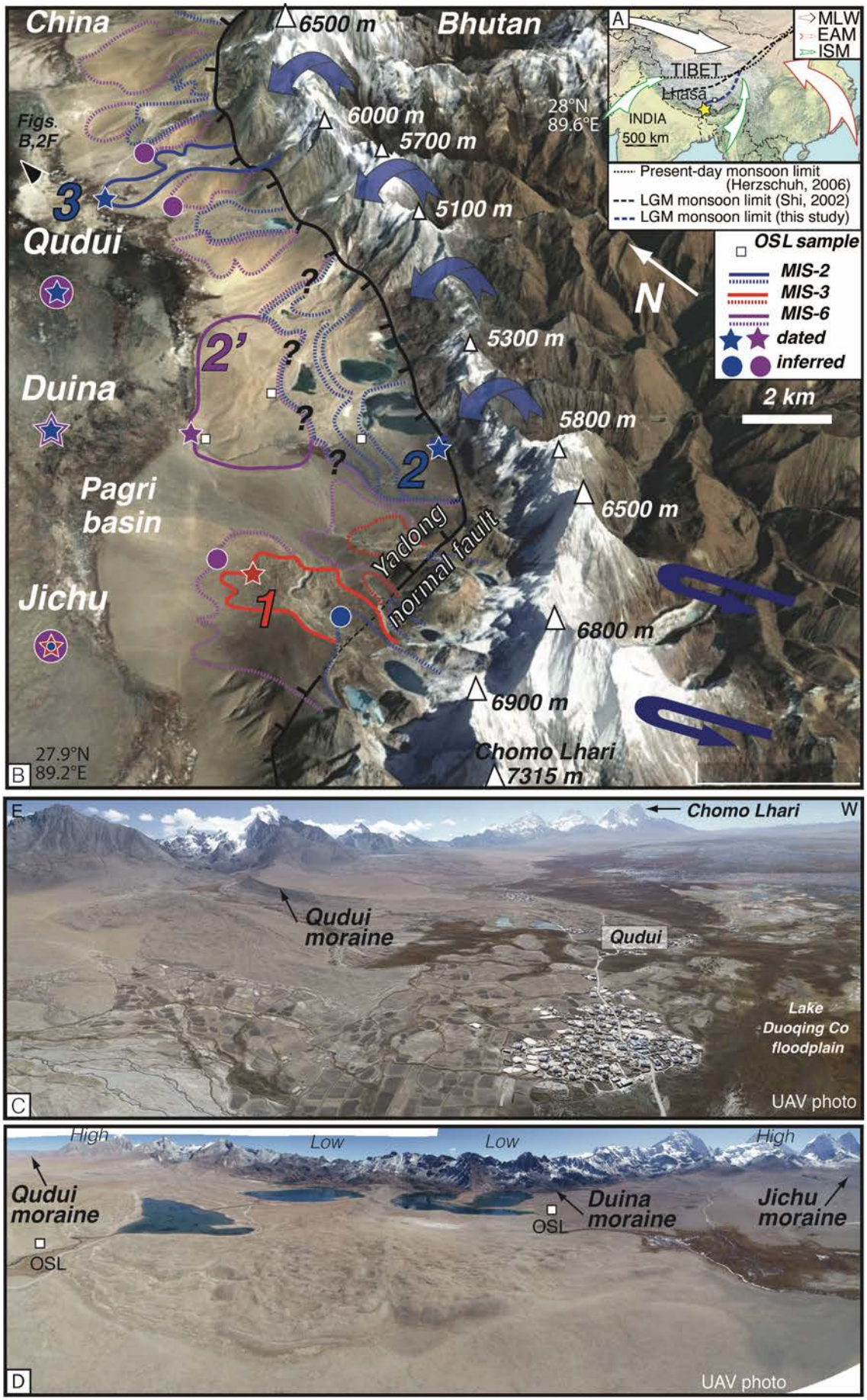
China
Bhutan
6500 m
6000 m
5700 m
5100 m
5300 m
5800 m
6500 m
6800 m
6900 m
Figs. B,2F
28°N 89.6°E
3
Qudui
2'
2
Duina
Pagri basin
1
Jichu
Yadong normal fault
Chomo Lhari 7315 m
27.9°N 89.2°E
B
A
MLW
EAM
ISM
TIBET
Lhasa
INDIA
500 km
Present-day monsoon limit (Herzschuh, 2006)
LGM monsoon limit (Shi, 2002)
LGM monsoon limit (this study)
OSL sample
MIS-2
MIS-3
MIS-6
dated
inferred
N
2 km
E
W
Chomo Lhari
Qudui moraine
Qudui
Lake Duoqing Co floodplain
UAV photo
C
High
Low
Low
High
Qudui moraine
OSL
Duina moraine
OSL
Jichu moraine
UAV photo
D

151

Figure 1: *Southern Yadong rift. (A) Location of Yadong rift (yellow star) within Asia, influenced by various climatic systems of Asia: mid-latitude Westerlies (MLW, black arrow), East Asian summer monsoon (EAM, red arrow), and Indian summer monsoon (ISM, green arrows). Dotted black line shows modern limit of monsoonal front (e.g., Herzschuh, 2006), while black (Shi, 2002) and blue (this study) dashed lines show that during the LGM. (B) Ages and names of dated (stars) and inferred (from local morphologic comparison, circles) moraines in southern Yadong rift in southern Tibet, located between highly incised slopes of Bhutanese Himalaya, and flatter Tibetan Plateau, shown on a 3D Google Earth view (approximate coordinates in corners). Dated Last Glacial Maximum (LGM, in blue) and Marine oxygen Isotope Stage (MIS)-3 (in red) are determined by ^{10}Be surface-exposure cosmogenic dating, while MIS-6 (in purple) are determined by Optically Stimulated Luminescence dating (OSL) (Ha et al., 2018, number #2' and white squares). The two moraines dated in this study are Jichu (#1) and Qudui (#3), while Duina (#2) has been dated by Wang et al. (2020) (Tables 1 and 2). Inferred LGM monsoonal precipitation shown by blue arrows - dark blue: precipitation blocked by highest peaks near Chomo Lhari summit (7315 m) at the base of which LGM moraines are small; light blue: abundant precipitation allowed by lower peaks (~5000-6000 m) near Qudui, where LGM moraines are large. (C) Unmanned Aerial vehicle (UAV a.k.a. drone) photograph of Qudui site with Chomo Lhari peak and Lake Duoqing Co floodplain. (D) UAV view of Duina site (location in B). Note low and high peaks along range. Location of two OSL samples (Ha et al., 2018) indicated by white squares.*

3. Material and methods

We used field investigation and Google Earth satellite imagery to map glacial landforms and select our sites in the Pagri basin of the southern Yadong rift. We collected 19 samples, seven at Qudui and 12 at Jichu, from the top few centimeters of large, stable, well-embedded granite boulders (1 to 4 m in diameter, Figs. S1 and S2) using chisel and hammer, located on lateral moraine crests at both sites, as well as on hummocky surfaces downstream at Jichu. We used cosmogenic ^{10}Be surface-exposure dating (e.g., Lal, 1991) to constrain the moraine abandonment ages (i.e., onset of deglaciation) following a procedure modified from Kohl and Nishiizumi (1992).

Ideally, one wants to sample boulders that have been exposed on moraine crests since

deglaciation, with no shielding, rolling or surface erosion since deposition (which tend to skew the ages toward values that are younger than the actual moraine age), and no exposure prior to deposition (which tends to skew occasional ages from the age distribution toward older values, e.g., Hallet and Pukonen, 1994; Putkonen and Swanson, 2003; Heyman et al., 2011). Despite moraines being relatively stable landforms over the long term, their crests can become unstable following glacier retreat, with large boulders being gradually exhumed to the surface as erosion washes the finer material away, thus with surface boulders representing multiple stages of exhumation as the surface lowers to a more stable position. It has been shown that erosion does not affect samples on young (≤ LGM), sharp, moraine crests as much as those located on sub-rounded MIS ≥6 moraine crests, as clearly observed in their respective age distribution: clustered ages with few outliers for LGM moraines, in contrast to continuous, scattered ages with no outlier for MIS-6 moraines (Chevalier and Replumaz, 2019). For that reason, one simply cannot accurately determine the abandonment age of a moraine older than the LGM from only a few individual boulder ages, but instead, one needs numerous individual boulder ages to determine the abandonment age of a particular moraine, as well as numerous moraine ages in order to examine the age distribution as a whole, and thus constrain the regional timing of glaciation (Chevalier and Replumaz, 2019; Balco, 2020). Note that we cannot emphasize enough how important it is to collect a sufficient number of samples on each moraine in order to increase the likelihood to date the actual age of a moraine (Chevalier et al., 2011). Our team is one of the few that dates a large number of samples per crest, ≥6 and often ≥10 (Table 2).

Ages were calculated using the CRONUS Earth calculator version 3 (Balco et al., 2008) using the St, Lm and LSDn production rate models as shown in Table 1, although we only refer to the Lm ages (Lal, 1991/Stone, 2000; time-dependent) throughout the paper. Topographic shielding was determined from Google Earth. We assumed zero erosion and did not correct for snow (unknown past snow cover data) and vegetation (absence of vegetation at both sites) covers, in

agreement with local studies (e.g., Owen et al., 2005; Liu et al., 2017), so that the apparent ages we calculate for each boulder may represent minimum ages. Statistical tests such as Peirce's criterion allow to identify and discard outliers from the age distribution of a particular moraine: one oldest sample at Qudui (14% of the population) and one oldest sample at Jichu (8%) (Table S1). Then, following Heyman (2014), we assign the Qudui and Jichu moraines to classes B (moderately-clustered) and C (poorly-clustered, as mainly observed for moraines older than the LGM, Chevalier and Replumaz, 2019), respectively, using reduced Chi-square analyses with internal (i.e., analytical), uncertainties (because all samples come from similar geographic setting so that their production rate is similar). We then take the oldest age of the distribution (after discarding outliers) to represent the emplacement age of the Qudui and Jichu moraines. Finally, to best assess whether MIS-3 moraines are more extensive than MIS-2 moraines in southern Tibet, we limit our regional age compilation (Table S2) to published studies which dated more than two samples from MIS ≥2 moraines (that excludes sites with erratics) using ^{10}Be cosmogenic surface-exposure dating, i.e., a total of 22 sites and 211 samples, including 159 from our team. Note that sometimes, the MIS age we allocate to certain dated deposits may differ from that given in the original publication (e.g., Payuwang and Ybj sites, see Supplementary material) due to differences in the production rate model or statistical analyses applied (Tables S1 and S2). Detailed description of the data used for the age compilation can be found in the supplementary material.

4. Site description and results

4.1. Qudui moraine

The NW-trending Qudui moraine originates from numerous glaciers in a large glacial cirque upstream, and consists of a single, large U-shaped valley (~1.5 km wide) bounded by sharp-crested lateral moraines downstream. Three young moraines limiting current glacial lakes are present far upstream in the valley, and two main debris-flow deposits (including one called DQ, Wang et al.,

2020), are confined within the main Qudui moraine (Fig. 2B). The Qudui moraine extends for ~7 km and almost reaches the current floodplain of Lake Duoqing Co (Figs. 1B and 2). The sharp, steep and high (~200 m) SW lateral moraine, and that, less steep and less high (<150 m) to the NE, with large lobate, hummocky deposits on its outer flank, lie on top of extensive, much smoother moraine surface remnants, visible as orange hues on satellite images, observed north and south of the Qudui valley (Figs. 1A and 2A,F). Fifteen km south of Qudui, similar deposits in the Duina area have been dated as MIS-6 (two ages, 135±21 and 181±25 ka, Ha et al., 2018) using Optically Stimulated Luminescence (OSL) dating (Fig. 1).

We collected a total of seven samples from the SW sharper, crest (C204-211), whose ages range from 20±2 to 41±3 ka (Figs. 2B, 3 and Table 1). The oldest age (C209) has been identified as a statistical outlier and was discarded (see methods section). The remaining ages are moderately-clustered (Class B moraine) and the oldest age (24±2 ka) is clearly LGM. An inner deposit (DQ, crossing the Yadong fault) has been dated by Wang et al. (2020) at 13±1 ka (recalculated oldest age, Table S2) using ^{10}Be dating (nine sample ages, no statistical outlier, Table S1), in agreement with its position within the LGM moraine (Fig. 2B-D). Similarly, the three sharp, inner moraines upstream must also be younger than the LGM (Fig. 2B-D).

Table 1: Analytical results of ^{10}Be geochronology and surface exposure ages of Jichu and Qudui moraines in the Yadong rift

Name	Lat (°N)	Long (°E)	Elev (m)	Quartz (g)	Shielding	Be carrier (mg)	^{10}Be/^{9}Be (10^-12)#	^{10}Be (10^6)at/g	St (years) §	Internal uncert. (yrs)	**Lm (years)§**	Internal uncert. (yrs)	LSDn (years) §	Internal uncert. (yrs)
Qudui moraine														
C204	28.06138	89.43633	4836	18.7757	0.994	0.2226	18.6749	1.4795±0.03	24076±1976	491	**22695±1774**	463	22573±1417	461
C205	28.06212	89.43575	4830	18.1260	0.994	0.236	18.3699	1.5987±0.0357	26099±2157	588	**24337±1917**	548	24221±1538	545
C206	28.06302	89.43523	4823	18.8365	0.973	0.2265	16.9312	1.3607±0.0315	22764±1885	530	**21697±1713**	505	21669±1381	504
C207	28.06435	89.43473	4802	19.9462	0.977	0.2437	18.006	1.4704±0.0307	24746±2035	521	**23245±1821**	490	23148±1458	487
C208	28.06511	89.43366	4784	18.2144	0.977	0.2449	15.245	1.3701±0.0263	23238±1901	449	**22035±1716**	425	21982±1372	424
C209	28.06619	89.43172	4753	19.1133	0.977	0.2456	30.3256	2.6048±0.0553	45059±3729	968	**40476±3188**	869	40291±2553	865
C211	28.06736	89.42472	4687	18.6321	0.976	0.2405	13.2389	1.142±0.0325	20241±1709	579	**19737±1592**	565	19863±1308	569
Jichu moraine														
Crest														
C101	27.89423	89.30846	5065	18.9897	0.978	0.2415	25.827	2.1951±0.049	33039±2736	744	**30037±2369**	676	29821±1896	671
C102	27.89737	89.30816	5047	15.8719	0.978	0.2476	17.379	1.8117±0.0394	27442±2265	602	**25411±1998**	557	25181±1594	552
C103	27.90011	89.3085	5022	9.8849	0.978	0.2357	8.5489	1.3625±0.031	20830±1722	477	**20241±1595**	463	20240±1287	463
C104	27.90303	89.30837	4987	15.6752	0.997	0.2387	11.9794	1.219±0.0282	18547±1534	432	**18351±1447**	427	18344±1168	427
Eastern hummocky deposit														
C106	27.91631	89.31726	4819	17.6505	0.989	0.2427	16.0811	1.4779±0.0312	24472±2014	521	**23016±1804**	490	22922±1445	488
C107	27.91916	89.31902	4773	17.1958	0.989	0.2356	8.0084	0.7334±0.0158	12361±1016	268	**13015±1019**	283	13033±822	283
C108	27.92141	89.3193	4734	17.4240	0.983	0.2481	6.9263	0.659±0.0149	11367±937	258	**12175±957**	277	12233±776	278
C110	27.92427	89.31915	4701	17.2629	0.983	0.2372	36.4167	3.3449±0.0505	59290±4843	909	**55567±4313**	851	54920±3393	841
Western hummocky deposit														
C111	27.92372	89.31061	4685	18.5931	0.98	0.2476	21.9473	1.9531±0.0303	34774±2825	545	**31745±2451**	497	31844±1959	498
C113	27.92234	89.30717	4703	17.4952	0.98	0.2333	18.6453	1.6617±0.0331	29302±2406	589	**26935±2105**	541	26889±1687	541
C115	27.91862	89.30649	4747	18.2415	0.98	0.2231	13.7341	1.1225±0.0255	19351±1599	443	**19012±1498**	435	19113±1215	438
C116	27.91874	89.30434	4729	17.9351	0.98	0.2398	30.279	2.7055±0.0406	47365±3856	720	**41888±3239**	636	41401±2548	628

Samples were processed at the Institute of Crustal Dynamics, China Earthquake Administration, Beijing (now called National Institute of Natural Hazards, Ministry of Emergency Management of China); and the $^{10}Be/^{9}Be$ ratios were measured at Xi'an AMS Center, China.

Ages are calculated with the CRONUS v3 calculator. St = Lal (1991)/Stone (2000) time-independent production rate model, Lm = Lal (1991)/Stone (2000) time-dependent production rate model,

LSDn = Lifton et al. (2014) production rate model.

All samples are granite (density is 2.7 g/cm^3); Thickness was taken as 5 cm. No erosion rate was applied.

Standards used at Xi'an AMS Center are '01-5-3' and '01-5-4' with ^{10}Be isotope ratios of $6.32x10^{-12}$ and $2.85x10^{-12}$, respectively, equivalent to 07KNSTD.

#Blank correction was applied with each 15 samples corresponding to a blank.

§ External Uncertainties (analytical and production rate, Balco et al., 2008) are reported at the 1σ confidence level.

251

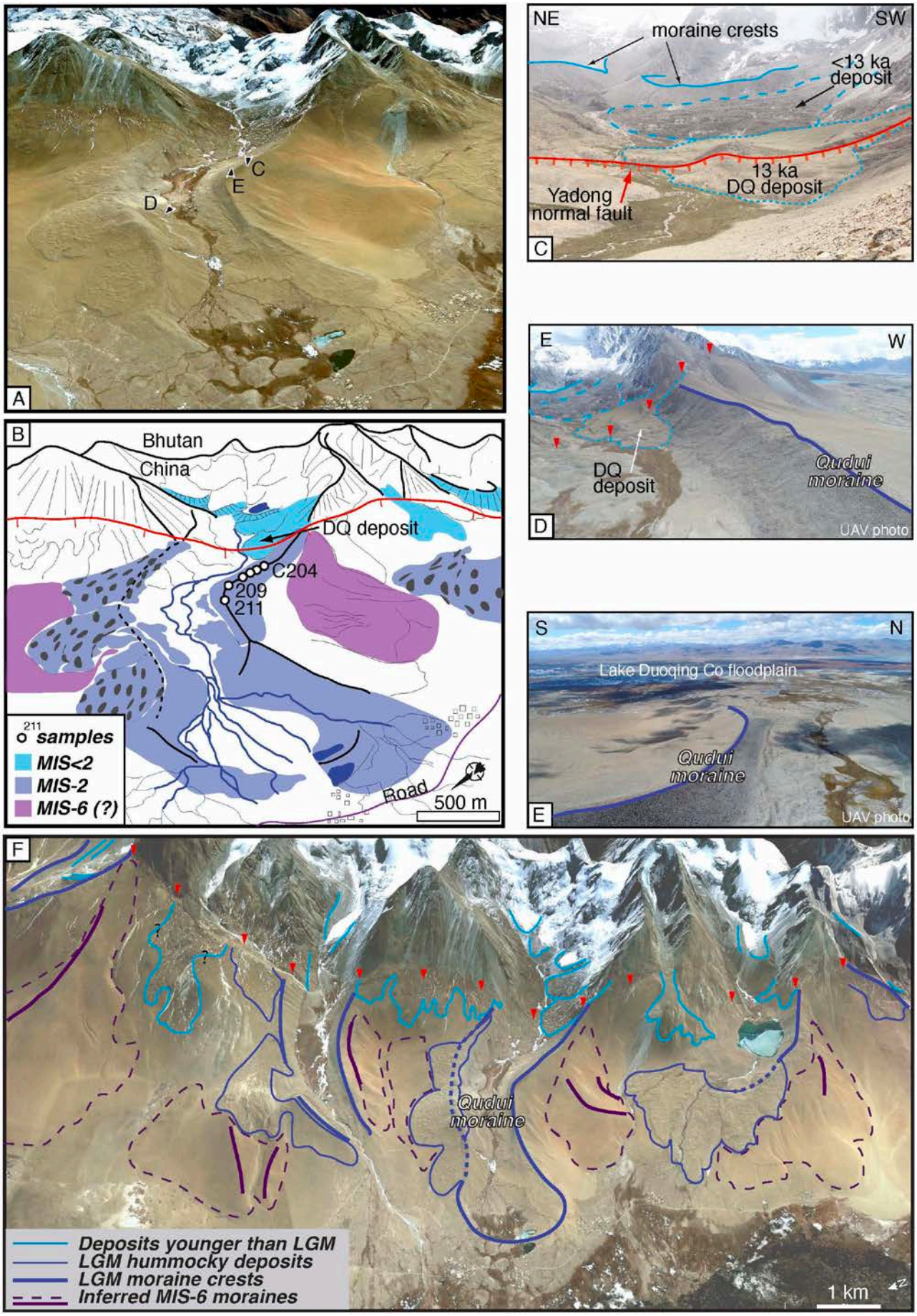
A
C
E
D
NE
SW
moraine crests
<13 ka deposit
13 ka DQ deposit
Yadong normal fault
C
E
W
DQ deposit
Qudui moraine
D
UAV photo
B
Bhutan
China
DQ deposit
C204
209
211
211 samples
MIS<2
MIS-2
MIS-6 (?)
Road
500 m
S
N
Lake Duoqing Co floodplain
Qudui moraine
E
UAV photo
F
Qudui moraine
Deposits younger than LGM
LGM hummocky deposits
LGM moraine crests
Inferred MIS-6 moraines
1 km

252

***Figure 2**: Qudui moraine site. (A,B) Google Earth image of Qudui moraine and its interpretation with samples location as white circles. Red line represents Yadong normal fault in B. (C) Field photograph of young (<LGM) deposits inset into Qudui moraine. Dotted, light blue line encompasses ~13 ka DQ deposit, which is vertically offset by Yadong normal fault (red line with tick bars) by ~11 m (Wang et al., 2020). Note additional moraines upstream (dashed and solid light blue lines). (D,E) UAV views of Qudui moraine crest with Lake Duoqing Co and its floodplain downstream. Red triangles indicate Yadong fault. (F) Google Earth image (location in Fig. 1A) of Qudui moraine and adjacent, most likely LGM deposits, on top of remnant, most likely MIS-6, moraine surfaces (orange hues, highlighted by purple dashed lines with crests in solid lines). Red triangles indicate Yadong fault.*

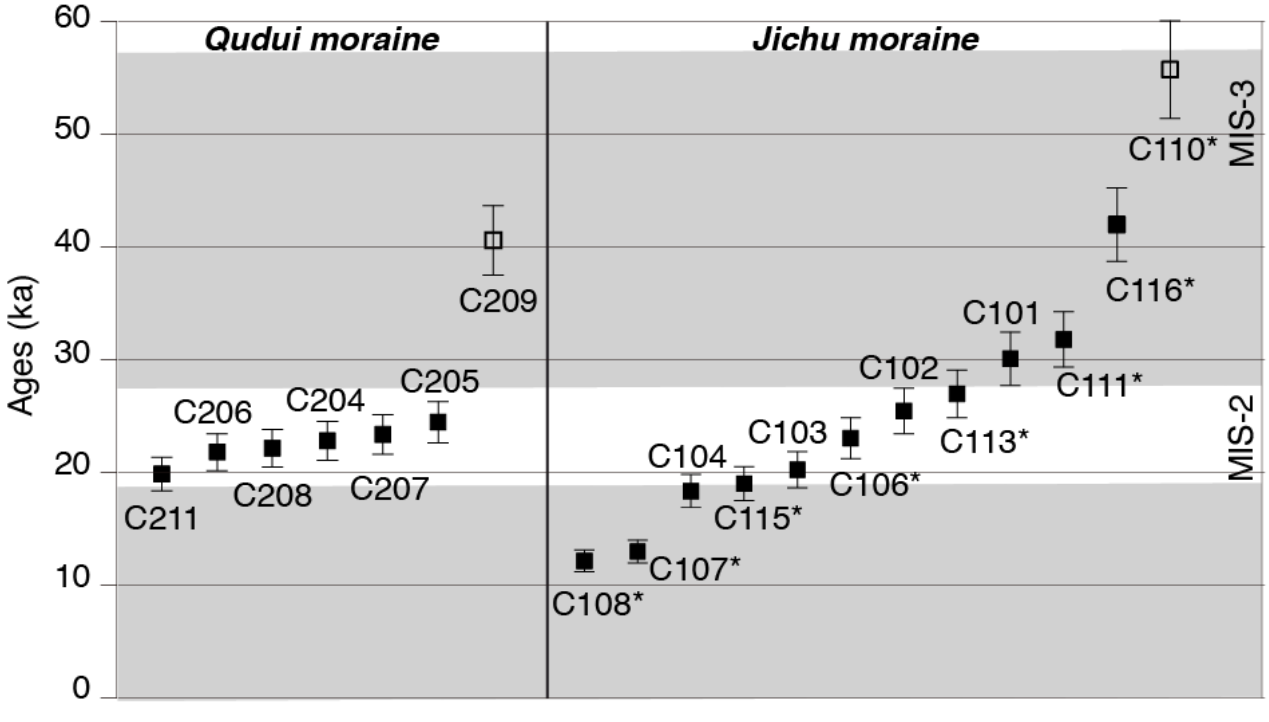

***Figure 3**: ^{10}Be cosmogenic surface-exposure ages of Qudui and Jichu moraines, using the 'Lm' Lal (1991)/Stone (2000) time-dependent model in CRONUS calculator v3 (Balco et al., 2008) with 1σ uncertainty. Numbers next to samples refer to sample names in Table 1. Outliers in white are discarded (using Peirce's criterion) when assigning a moraine age (see methods section). Grey sectors represent Marine oxygen Isotope Stages (MIS). Note the difference in age spread between samples collected from hummocky (* symbol, ages more scattered) deposits at Jichu and the lateral Jichu and Qudui crests (more clustered).*

4.2. Jichu moraine

The Jichu moraine complex is one of the largest in the entire Pagri basin, with three large glacial cirques from which large glaciers flow northward, and where several present-day, ~1 km-long, glacial lakes exist, each surrounded by several sharp moraine crests (light blue in Fig. 4A-C). Downstream and outside of these frontal moraines, relatively sharp crests (dark blue in Fig. 4) reach the Jichu U-shaped valley, with clear breach of their frontal crest (Fig. 4C). The largest moraine, Jichu, which extends ~7.6 km from the current glacier snout located at ~5100 m, consists of lateral crests (sharper to the west) surrounded by hummocky deposits to the east and front. These Jichu deposits also lie on top of extensive, much smoother moraine surface remnants (Fig. 4A,B) which may also be inferred to belong to MIS-6 by comparison with the two OSL ages from the smooth surfaces downstream from Duina (Fig. 1).

We collected a total of 12 samples at the Jichu site: four samples (C101-104) from the sharp and linear lateral, western crest upstream, and eight samples (C106-116) from the hummocky deposits downstream (Fig. 4B). Ages are scattered from 12±1 to 56±4 ka (Fig. 3 and Table 1). Note that ages on the hummocky surfaces are more scattered (ranging from 12 to 56 ka) than those on the moraine crest (18 to 30 ka). The oldest age (C110 at 56 ka) has been identified as a statistical outlier (see methods section). The deposits (moraine crest and hummocky surfaces) are Class C (taken together or separately, Table S1) so that the oldest age is taken to represent their abandonment age, i.e., MIS-3 (with or without discarding outlier). Considering no outlier, as observed for moraines older than the LGM in SE Tibet (Chevalier and Replumaz, 2019), and as explained in the methods section, Jichu is assigned to early MIS-3.

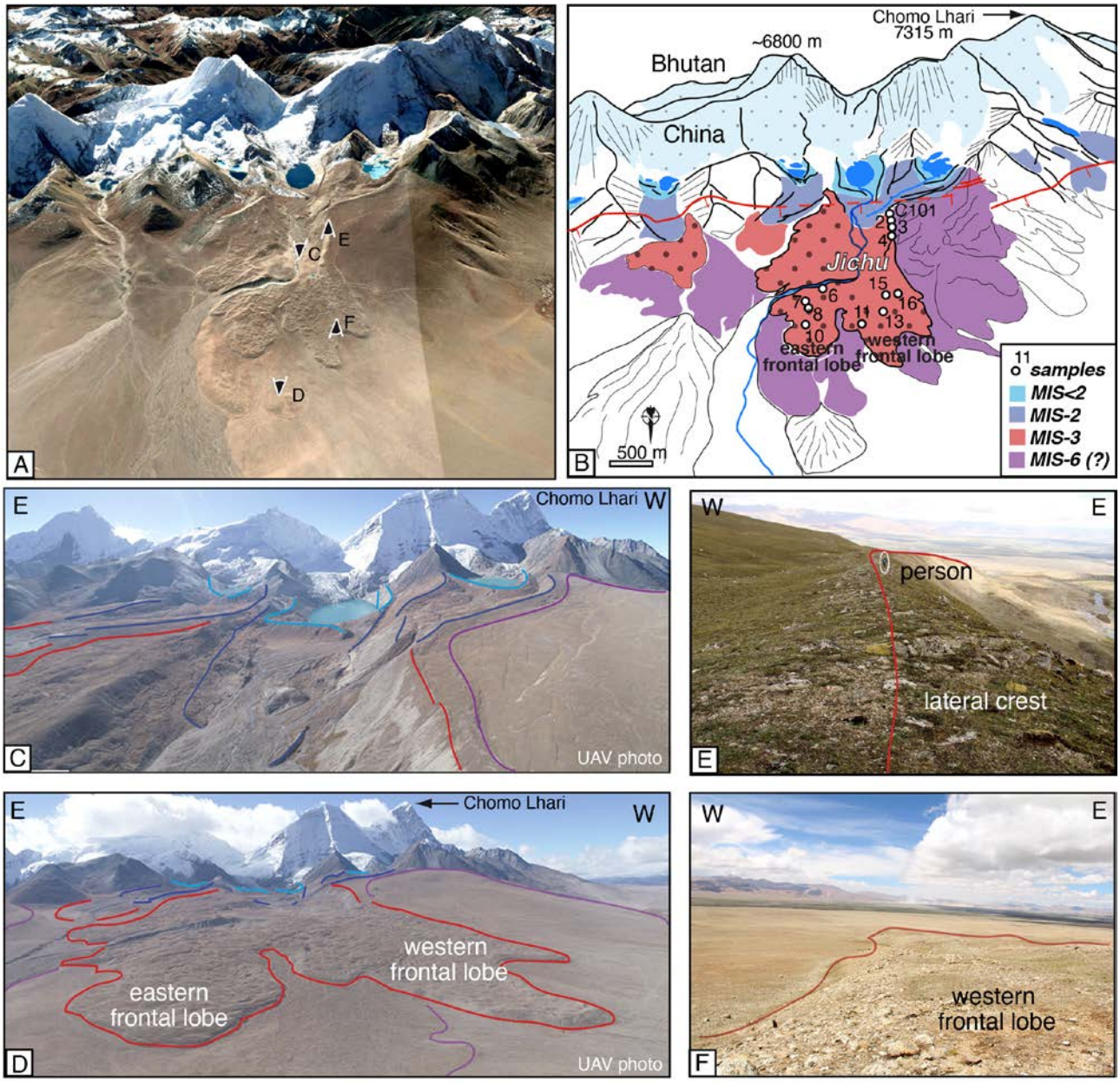

Figure 4*: Jichu moraine site. (A,B) Google Earth image of Jichu moraine and its interpretation with samples location as white circles. Red line with tick bars in B represents Yadong normal fault. (C,D) UAV photographs of moraines and hummocky deposits, respectively, with crests highlighted by colors according to their ages (legend in B). (E) Field photograph of the western, lateral Jichu crest. (F) Field photograph of hummocky deposit downstream.*

5. Discussion

5.1. Past glacial advances at Qudui and Jichu

Surprisingly, the age distribution of the two largest, imbricated moraines we study at Qudui and Jichu, both located in the Pagri basin of the southern Yadong rift, is very different despite their close proximity (~20 km) (Fig. 1A). At Qudui, the largest and sharpest moraine shows tightly clustered ages between 20 and 24 ka with one statistical outlier at ~40 ka. Such clustering allows to firmly conclude that the Qudui moraine belongs to the LGM, as observed all around Tibet (e.g., Owen and Dortch, 2014; Chevalier et al., 2011; Chevalier and Replumaz, 2019). The Qudui moraine lies on top of more extensive, older, smoother remnant moraine surfaces, with partly preserved, sub-rounded crests (orange hues on satellite images, purple in Fig. 2F). Similar surfaces located downstream from the Duina moraine south of Qudui (#2' in Fig. 1A) have been dated as MIS-6 with two OSL samples (Ha et al., 2018).

By contrast, the Jichu moraine ages are scattered and continuous from 12 to 56 ka, that we interpret as MIS-3 considering the oldest ages of the scattered age distribution as representative of the age of the moraine, as observed for moraines older than the LGM (Chevalier and Replumaz, 2019). Whether the oldest sample is an outlier does not affect the moraine's MIS assignment. The Jichu moraine also lies on top of moraine surfaces similar to those observed regionally and dated as MIS-6 (Figs. 1A and 4). Much sharper, although smaller, moraine crests are observed upstream, closer to the glacial lakes and are most likely LGM and younger (dark and light blue, respectively, Figs. 1A and 4B,C).

In summary, extensive LGM moraines lie directly on top of presumably MIS-6 moraines at Qudui, with no MIS-3 deposits in between. At Jichu by contrast, extensive MIS-3 moraines rest directly atop most likely MIS-6 moraines, with less extensive LGM moraines located upstream within the MIS-3 deposits (Fig. 1A). Therefore, we infer that while the most extensive moraines in the southern Yadong rift may be MIS-6 everywhere, the relative extent of MIS-3 and MIS-2

moraines varies at places, depending on the elevation of the surrounding peaks, that influences local precipitation, as further explained below.

5.2. Influence of temperature and precipitation

Both moraines originate from the western side of the Chomo Lhari Range, uplifted by the Yadong normal fault and forming a topographic boundary between China and Bhutan (Fig. 1A). However, despite only being ~20 km apart, their topographic setting is different, with the Jichu site located at the base of the highest summits (~7000 m) while Qudui is located at the base of lower summits (<6000 m), just north of a series of even lower summits (~5000 m) (Fig. 1). We thus infer that these two sites may have received different amounts of monsoonal summer precipitation from Bhutan, with Jichu lying in a rain shadow behind the highest peaks acting as a topographic barrier, while precipitation could more easily reach the Qudui moraine thanks to the lower elevation of the nearby summits (blue arrows, respectively, Fig. 1A). Therefore, although the LGM period was very cold and arid (temperature 6-9°C and precipitation 30-70% lower than today, e.g., Shi, 2002), with low monsoon intensity (Wang et al., 2008) hence low effective moisture (Herzschuh et al., 2006) and minimum insolation (Berger and Loutre, 1991), we infer that the lower summits near Qudui nevertheless allowed precipitation to reach the Pagri basin, hence favoring LGM glacier advance now visible as the large LGM Qudui moraine and its neighbors. By contrast, in spite of similar low temperature conditions during the LGM near the high summits of the Chomo Lhari Range at Jichu, sufficient to sustain glaciers growth, its location shielded from LGM precipitation prevented large LGM advances, as now observed upstream at Jichu as restricted LGM moraines (Figs. 1A and 4). At Jichu, the MIS-3 moraine is much more extensive than the LGM moraines, despite the fact that MIS-3 was warmer (2-4°C higher than today, Shi, 2002) than the LGM period but with more intense moisture (40-100% higher than today, e.g., Shi, 2002; Herzschuh, 2006) that brought more snowfall at the highest elevations (e.g., Finkel et al., 2003), hence allowing larger glaciers to grow and larger MIS-3 moraines to be deposited at the base of the highest summits.

353 At Jichu, we have dated both the western, well-preserved crest, as well as the hummocky
354 deposits downstream from it, with scattered ages between ~10 and 55 ka (Fig. 3). As shown in our
355 regional compilation of southern Tibet (Fig. 5), and in that of eastern Tibet (Chevalier and
356 Replumaz 2019), such scattered age distribution with several ages older than the LGM (here 4 out
357 of 12, i.e., 33% for Jichu), clearly indicates that deposition occurred prior to the LGM. Such highly
358 lobate, hummocky morphology, observed at Jichu and at numerous places in the Yadong rift, may be
359 due to extensive ice-avalanche/glacier-derived debris flows, that may have been triggered by
360 earthquakes on the Yadong fault. Interestingly, the fact that, in general, the right bank of the glacial
361 valleys displays such hummocky surfaces rather than the left bank, which seems intact with well-
362 preserved, well-defined moraine crests (such as those we sampled at Qudui and Jichu), may be due
363 to valley curvatures. The limited extent of such ice-avalanches, 'spilling' over the main moraine
364 crest rather than spreading far down the foreland basin, may reflect their somewhat viscous, more
365 ice-based than water-based nature. This suggests that these hummocky deposits most likely occurred
366 toward the end of glacial periods when the climate was still cold, with sufficient ice left in the valley
367 and limited water accumulation within glacial lakes, rather than during interglacials. This is indeed
368 what we observe at Jichu, where both the hummocky deposits and the main crest have been dated as
369 MIS-3.
370 One OSL sample was collected at depth, below the hummocky surfaces (because OSL dating
371 requires collecting samples that have been protected from light after deposition) between the
372 upstream Duina moraine (which is LGM, Wang et al., 2020, #2 in Fig. 1A) and the MIS-6 remnant,
373 smooth surfaces (#2', Fig. 1A,C), and its age is MIS-5/6 within uncertainties (129±21 ka, Ha et al.,
374 2018). However, because hummocky deposits are not uniformly thick, we speculate that this sample
375 may be overestimated because it may have been collected, for example, in a low zone, i.e., dating
376 what lies underneath it. Instead, we infer that the series of intermediate surfaces surrounding large,
377 present-day glacial lakes (dashed blue lines in Fig. 1A) most likely belong to the LGM, representing

successive, recessional moraines, the latter (most recent) of which is the Duina moraine, which was eventually abandoned at ~17 ka past the Yadong fault (Wang et al., 2020). Additional ^{10}Be samples would clearly be necessary to assess this discrepancy.

In summary, we suggest that while climatic conditions during the LGM were sufficient to sustain glaciers growth everywhere in the Chomo Lhari Range region thanks to low temperatures, 1) glaciers shielded from limited LGM precipitation only slightly advanced, such as near the high summits at Jichu, where only restricted LGM moraines exist (Figs. 1A and 4); and 2) glaciers that received more LGM precipitation thanks to lower summits, as observed near Qudui, show extensive LGM moraines. By contrast, we suggest that MIS-3 moraines were able to be deposited at the base of the highest summits thanks to intense precipitation which brought abundant snowfall at high elevations despite global temperatures warmer than during the LGM. Lastly, MIS-6 being the coldest period in recent climate history (e.g., Lisiecki and Raymo, 2005), such glacial advances occurred all along the southern Yadong rift (Fig. 1A).

5.3. Age compilation shows limit of LGM monsoonal precipitation

To further assess the relative extent of MIS-2 and MIS-3 glacial advances elsewhere in southern Tibet, we compiled ages (Fig. 5, Tables 2 and S2, plus details on each study in the Supplementary material) of the most extensive moraines from regional studies north of the eastern Himalayas from three ~N-S transects of ~400, ~300 and ~50 km-long, from the Himalaya to central Tibet: the Yadong-Gulu, Dinggye-Xainza, and Kung Co transects, respectively, from east to west (Fig. 6). This compilation allows to assess whether timing and extent of glaciations may have varied in a N-S and/or E-W direction, due to variations in topography and amounts of precipitation.

The compilation clearly shows very different individual boulder age distributions: clustered ages with few outliers for MIS-2 moraines and scattered but continuous ages for moraines older than the LGM (Fig. 5). This clearly distinct distribution pattern has already been observed in a similar compilation from eastern Tibet, interpreted as limited erosion on young (LGM) moraine

crests which remain sharp with numerous boulders on top, while erosion strongly affected sub-rounded, older moraine crests with fewer boulders on top, showing a scattered but continuous age distribution with oldest ages being MIS-6 (Chevalier and Replumaz, 2019). Similarly, here, the oldest ages in the scattered age distributions fall into MIS-6 and correspond to widely observed smooth surfaces, visible as orange hues on satellite images (Figs. 1A and 2F). Ages older than MIS-6 have been obtained occasionally on highly degraded moraines (Owen et al., 2009; Chevalier et al., 2011). These oldest surfaces, preserved in specific settings which need to be studied in more details, are beyond the scope of this paper, hence are not shown in the compilation. Therefore, as documented in more humid eastern Tibet (Chevalier and Replumaz, 2019), as well as in arid central Tibet (Schafer et al., 2002; Owen et al., 2005), the MIS-6 moraines are observed throughout Tibet. Indeed, our compilation and that of Chevalier and Replumaz (2019) show uniform MIS-6 ages of the most extensive moraines in southern and eastern Tibet, respectively, rather than a northward increase of their age, from more humid southern Tibet to more arid central Tibet, as previously suggested (Owen et al., 2005; Owen and Dortch, 2014).

Following Chevalier and Replumaz (2019)'s approach, we suggest that the oldest ages from numerous scattered, continuous age distributions from moraines older than the LGM best represent the age of such moraines. Too often, moraines with scattered age distribution are simply disregarded and MIS are not allocated (e.g., Blomdin et al., 2018), hence no new data are added to the growing database, and no contribution to the debate on which age best represents the actual moraine age can be made. Indeed, such moraines older than the LGM are harder to date, and more samples are needed to estimate their abandonment age (≥6 samples, Chevalier et al., 2011), to eventually reconstruct past glaciations that recorded past changes in atmospheric circulation, precipitation and temperature, i.e., past climatic changes.

Between the clustered ages of MIS-2 moraines and the scattered but continuous ages of MIS-6 moraines, i.e., narrow *vs* broad probability density function (pdf) peaks, respectively, the

compilation shows intermediate pdf widths, such as MIS-3 for Jichu (Fig. 5). Such MIS-3 advances are clear and have commonly been observed in Tibet (e.g., Owen et al., 2002, 2010; Finkel et al., 2003; Hedrick et al., 2011). While the MIS-3 pdf peak is wider than that of the LGM, it is much less broad than that of MIS-6 (Fig. 5). Interestingly, some sites show age distributions with slightly older oldest ages at MIS-4 with an even broader pdf peak (Fig. 5), suggesting MIS-4 advances (see review by Doughty et al., 2021). Further dating would be necessary to advance on this topic, which is beyond the scope of this paper, as the two sites we study here do not show such MIS-4 ages.

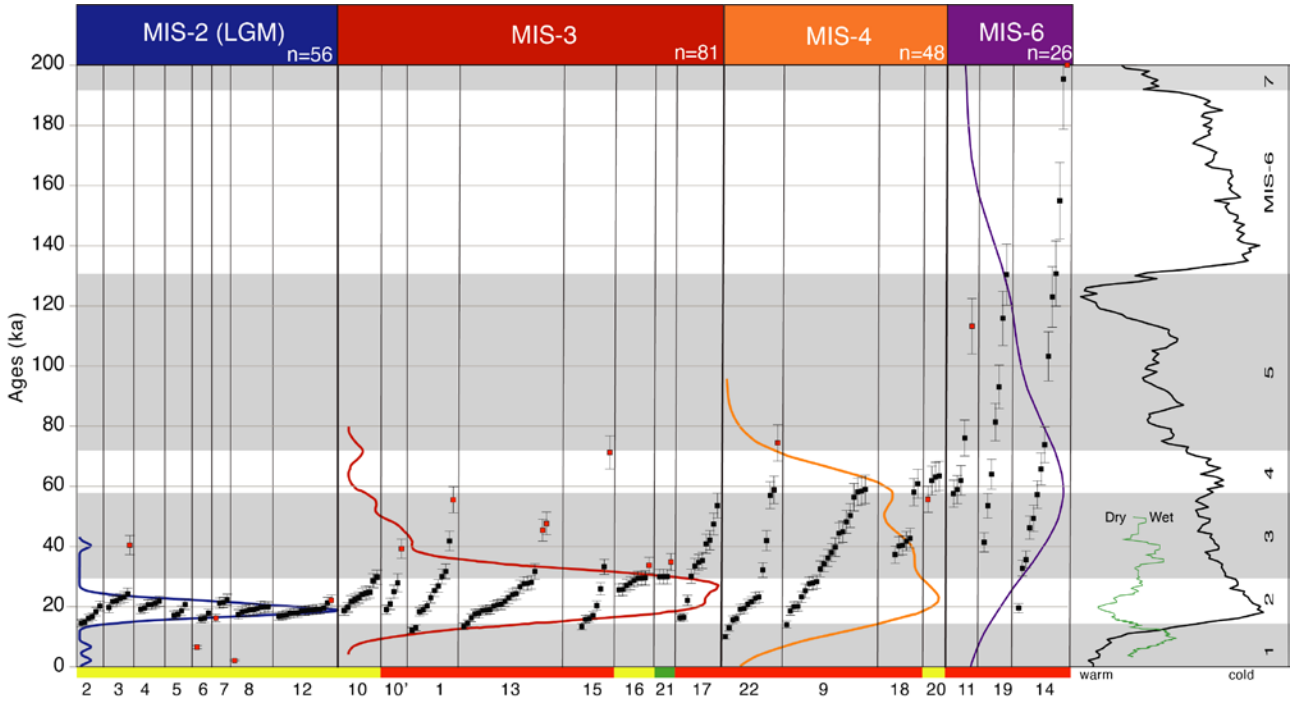

Figure 5*: Age compilation (recalculated as ages in Fig. 3) of most extensive moraines between Marine oxygen Isotope Stages (MIS)-2 and MIS-6 in southern Tibet (Yadong-Gulu, Dinggye-Xainza and Kung Co rifts). Samples in red are outliers rejected by Peirce's criterion (Table S1). We classified moraines per MIS ages according to their oldest ages, excluding outliers (Table 2) as well as plotted probability density functions (pdfs) within each MIS group. Vertical lines separate different studies with corresponding numbers at bottom as in Figures 1, 6, Table 2 and Suppl. To the right, global climatic proxy curve of Lisiecki and Raymo (2005) in black, effective moisture (Herzschuh, 2006) in green, and gray-shaded sectors showing MIS. Colors at bottom refer to well-clustered (green, Class A), moderately-clustered (yellow, B) and poorly-clustered (red, C) moraine ages distribution, obtained using reduced Chi-square analyses (Heyman, 2014) (Table S1).*

446 **Table 2.** Compilation of most extensive, pre-LGM moraine ages from southern Tibet

Site name	# in Figs. 1 and 5	Lat-Long (°N - °E)	Reference	Number of samples	Outliers rejected ‡	Moraine class	Age (ka)†	MIS assignment	Elev. of highest peak (m)
Yadong rift									
Jichu	1	27.91 - 89.3	**This study**	12	1 old	C	42±3	MIS-3	6800-7300
Duina	2	27.92 - 89.38	Wang et al. (2020)	6	/	B	20±2	LGM	5100-5300
Downstream Duina	2'	27.97 - 89.34	Ha et al. (2018)	/	/	/	/	MIS-6 (OSL ages)	5100-5300
Qudui	3	28.06 - 89.43	**This study**	7	1 old	B	24±2	LGM	5500-6000
Cogarbu M5	4	28.3 - 89.9	Peng et al. (2019)	6	/	B	22±2	LGM	5500-6300
Karola	5	28.89 - 90.25	Owen et al. (2005)	4	/	B	21±2	LGM	6000-6300
M4W	6	28.97 - 90.12	Liu et al. (2017)	4	1 young	B	18±1	LGM	6500-7200
M4E	7	28.9 - 90.25	Liu et al. (2017)	4	1 young	B	22±2	LGM	7200 (E of the range)
N Yadong-Gulu rift									
Quemuqu	8	29.85 - 90.06	Dong et al. (2017)	10	1 young	B	20±2	LGM	7000 (E of the range)
Ybj	9	30.02 - 90.24	Chevalier et al. (2011, 2020)	22	/	C	59±5	MIS-4	6000 (E of the range)
Payuwang inner	10	30.61 - 90.76	Dong et al. (2014)	10	/	B	30±2	MIS-3	5800
Payuwang outer	10'	30.61 - 90.76	Dong et al. (2014)	5	1 old	C	28±3	MIS-3	5800
Gulu south	11	30.76 - 91.58	Owen et al. (2005)	5	1 old	C	76±6	inferred MIS-6*	5900-6200 (E of the range)
Gulu	12	30.8 - 91.56	Chevalier et al. (2011, 2020)	15	1 old	B	21±2	LGM	6600 (E of the range)
Dinggye rift									
Dinggye S	13	28.14 - 87.66	Chevalier et al. (2011)	22	2 old	C	32±3	MIS-3	6200-6400
Dinggye N	14	28.31 - 87.73	Chevalier et al. (2011)	14	1 old	C	195±17	MIS-6	5800-6100
Xainza rift									

M	15	29.81 - 88.2	Chevalier et al. (2011)	8	1 old	C	33±3	MIS-3	6000-6200
M1	16	29.92 - 88.3	Chevalier et al. (2011)	9	1 old	B	30±2	MIS-3	6000
M2	17	30.09 - 88.4	Chevalier et al. (2011)	11	/	C	54±4	MIS-3	5800
M3 main	18	30.59 - 88.51	Chevalier et al. (2011)	7	/	C	61±5	MIS-4	6000 (E of the range)
M4	19	30.64 - 88.56	Chevalier et al. (2011)	7	/	C	130±10	MIS-6	6000 (E of the range)
Mt Jaggang JM1	20	30.82 - 88.71	Dong et al. (2018)	4	1 young	A	63±5	MIS-4	6500 (E of the range)
Kung Co rift									
Cho Oyu	21	28.35 - 86.63	Chevalier et al. (2011)	4	1 old	A	30±0.03	MIS-3	8200 (Himalayan moraine)
	22	28.77 - 86.46	Chevalier et al. (2011)	15	1 old	C	59±5	MIS-4	5900

‡Outliers rejected using Peirce's criterion. †Average age if Class A, oldest age if Classes B and C (Heyman, 2014).

** See supplementary text for details*

Interestingly, the spatial distribution of the MIS-3 or MIS-4 moraines (Fig. 6) suggests that they are located mostly west and north of the Yadong rift, at the base of high regional peaks (>5800 m, Table 2) such as the Chomo Lhari (Jichu moraine). By contrast, in the Yadong rift, LGM moraines are located at the base of both high and low summits (between 5100 and 7200 m, Table 2), but are larger where LGM precipitation are abundant such as near the low (~5000 m) Karola pass or at Qudui. Indeed, considering that temperature was most likely broadly similar in the entire study region at a given period, the fact that LGM moraines appear more extensive in the Yadong rift than anywhere else at similar elevation may reflect a strong link to precipitation. Therefore, while low temperature during the LGM allowed glaciers to advance at most places on the Tibetan Plateau, LGM moraines seem more extensive at places where LGM precipitation could reach, such as at Qudui and in the northern Yadong rift via the low Karola pass, rather than being blocked by high summits (such as at Jichu) or being located too far from the monsoonal front, such as farther north (N Yadong-Gulu rift) and west (Dinggye-Xainza and Kung Co rifts) (Fig. 6). There, away from the

LGM monsoonal front, LGM moraines are less extensive than older moraines (MIS-3 or MIS-4), suggesting that in more arid regions, moraines older that the LGM are preserved thanks to less extensive advance of LGM glaciers. Therefore, the relative spatial distribution of LGM *vs* MIS-3/4 moraines shown by our compilation allows to tentatively draw new limits of monsoonal precipitation during the LGM (Fig. 6).

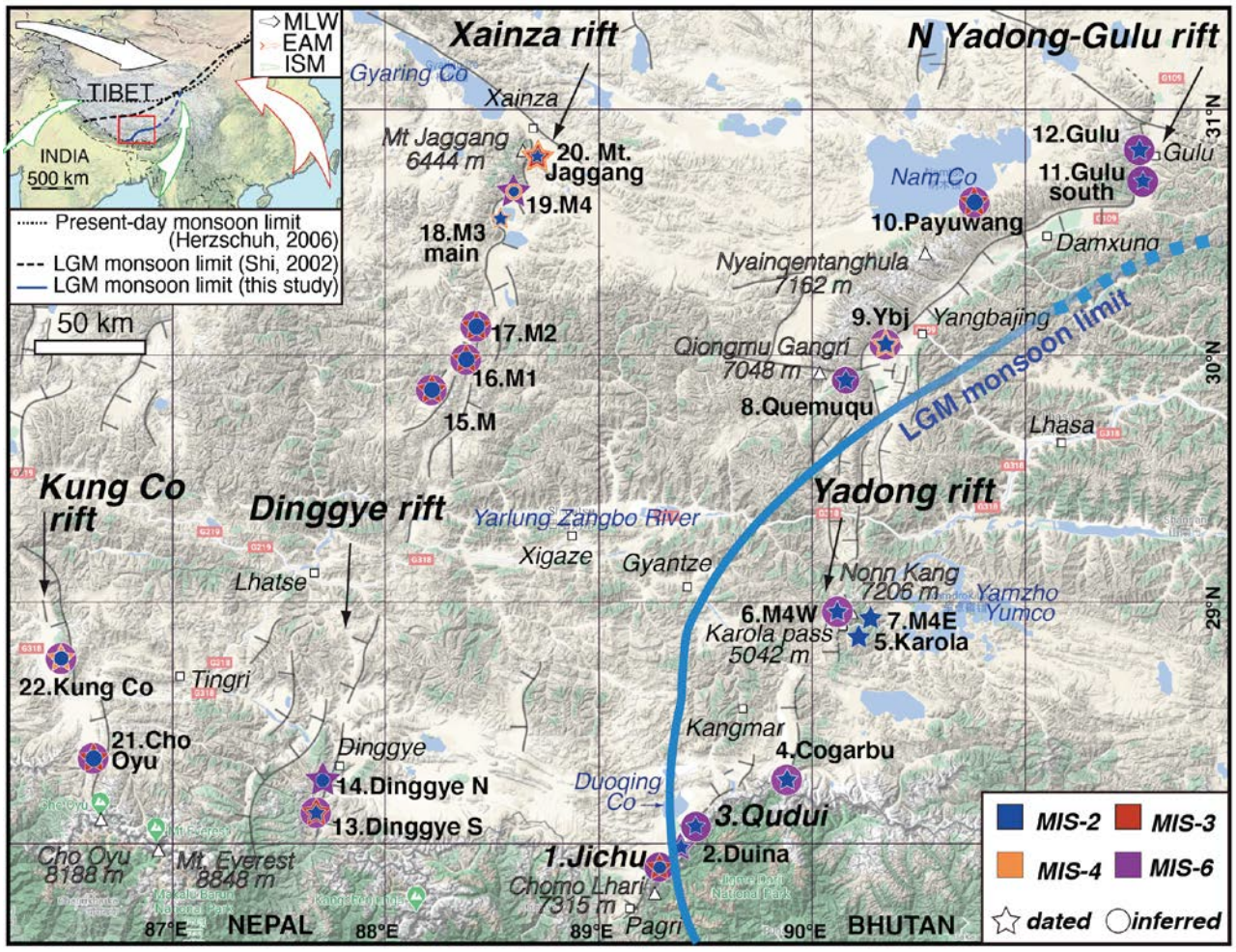

Figure 6: *Compilation of moraine ages from southern Tibet (numbers and names of sites as in Table 2). Details of each study can be found in supplementary material and Table S2. Stars indicate dated moraine ages while circles indicate inferred ages, with colors according to their MIS as in legend. Main cities and towns, mountain peaks and geographic landmarks (lakes and rivers) are indicated. Yadong-Gulu, Dinggye-Xainza and Kung Co rifts are bounded by active normal faults represented as grey lines with tick bars. We suggest a new LGM monsoonal precipitation front as represented by thick blue line (see text for details). Inset as in Figure 1A.*

6. Conclusion

By studying two moraines in the southern Yadong rift in southern Tibet, Qudui and Jichu, and compiling the ages of the most extensive moraines from three N-S transects from southern to central Tibet (22 sites, 211 ^{10}Be samples), we suggest that:

1) the limit of monsoonal precipitation during the last glacial maximum (LGM, 19-26.5 ka) can be determined considering that LGM moraines extend farther than MIS-3 moraines where LGM monsoonal precipitation were able to reach. Indeed, during MIS-3, large glaciers advanced from high summits (≥5800 m) thanks to the large increase in precipitation (hence snowfall) at high elevation despite temperature warmer than during the LGM. During MIS-2 however, glacier growth was sustained all over Tibet even from lower summits (≥5100 m) thanks to colder temperature, but their extent spatially varied depending on the amount of monsoonal precipitation received during that period. At places easily reached (absence of topographic barrier or closer to the monsoonal precipitation front), MIS-2 moraines are the most extensive (such as at Qudui). By contrast, away from the monsoonal front or where LGM precipitation was blocked by topographic barrier (such as at Jichu), MIS-2 advances were limited and MIS-3 advances were preserved downstream. Overall, MIS-6 moraines are the largest deposits in most places in Tibet, including in more humid regions such as the Tibetan Himalaya or eastern Tibet, as well as in more arid regions such as central Tibet.

2) Glaciers from the Yadong-Gulu region, located in a climatic transition zone between the mid-latitude Westerlies and the monsoon, are thus sensitive to both variations in temperature and precipitation. Detailed study of imbricated moraines that record successive past glacial advances allows to study changes in atmospheric circulation, precipitation and temperature, as well as to reconstruct paleoclimate, and advance our understanding on the LGM monsoonal precipitation limit.

Acknowledgements

This project was financially supported by the Second Tibetan Plateau Scientific Expedition of the Ministry of Science and Technology of China [2019QZKK0901], the National Natural Science Foundation of China [42020104007, 41941016], the China Geological Survey [DD20190059]. All data are found in Tables 1, 2, S1 and S2.

References

Armijo, R., Tapponnier, P., Mercier, J.L., Han, T.L., 1986. Quaternary extension in southern Tibet: Field observations and tectonic implications. Journal of Geophysical Research, 91, 13,803 – 13,872.

Balco, G., Stone, J.O., Lifton, N.A., Dunai, T.J., 2008. A complete and easily accessible means of calculating surface exposure ages or erosion rates from 10Be and 26Al measurements. Quaternary Geochronology, 8, 174–195.

Balco, G., 2020. Glacier Change and Paleoclimate Applications of Cosmogenic-Nuclide Exposure Dating, Annual Review of Earth and Planetary Sciences, 48, 21-48, doi: 10.1146/annurev-earth-081619-052609.

Benn, D.I., Owen, L.A., 1998. The role of the Indian summer monsoon and the mid-latitude westerlies in Himalayan glaciation: review and speculative discussion. Journal of the Geological Society, London, 155 (2), 353-363.

Berger, A., Loutre, M.F., 1991. Insolation values for the climate of the last 10 million years. Quaternary Science Reviews, 10, 297–317.

Blomdin, R., Stroeven, A.P., Harbor, J.M., Gribenski, N., Caffee, M.W., Heyman, J., et al., 2018. Timing and dynamics of glaciation in the Ikh Turgen Mountains, Altai region, High Asia. Quaternary Geochronology, 47, 54-71, doi:10.1016/j.quageo.2018.05.008.

524 Bookhagen, B., Burbank, D.W., 2006. Topography, relief, and TRMM-derived rainfall variations
525 along the Himalaya, Geophysical Research Letters, 33, L08405,
526 doi:10.1029/2006GL026037.
527 Chevalier, M.L., Hilley, G., Tapponnier, P., Van DerWeord, J., Liu-Zeng, J., Finkel, R.C.,
528 Ryerson, F.J., Li, H., Liu, X., 2011. Constraints on the late Quaternary glaciations in Tibet
529 from cosmogenic exposure ages of moraine surface. Quaternary Science Reviews, 30, 528–
530 554. doi:10.1016/j.quascirev.2010.11.005.
531 Chevalier, M.L., Leloup, P.H., Replumaz, A., Pan, J., Liu, D., Li, H., Gourbet, L., Metois, M., 2016.
532 Tectonic-geomorphology of the Litang fault system, SE Tibetan Plateau, and implication for
533 regional seismic hazard ; Tectonophysics, 682, 278-292, doi:10.1016/j.tecto.2016.05.039.
534 Chevalier, M.L., Replumaz, A., 2019. Deciphering old moraine age distributions in SE Tibet
535 showing bimodal climatic signal for glaciations: Marine Isotope Stages 2 and 6. Earth and
536 Planetary Science Letters, 507, 105-118, doi:10.1016/j.epsl.2018.11.033.
537 Chevalier, M.L., Tapponnier, P., van der Woerd, J., Leloup, P.H., Wang, S., Pan, J., Bai., M., Kali,
538 E., Liu, X., Li, H., 2020. Late Quaternary Extension Rates Across the Northern Half of the
539 Yadong-Gulu Rift – Implication for East-West Extension in Southern Tibet. Journal of
540 Geophysical Research, 125, e2019JB019106, doi:10.1029/2019JB019106.
541 Clark, P.U., Dyke, A.S., Shakun, J.D., Carlson, A.E., Clark, J., Wohlfarth, B., Mitrovica, J.X.,
542 Hostetler, S.W., McCabe, A.M., 2009. The last glacial maximum. Science, 325, 710-713.
543 Dong, G.C., Yi, C.L., Caffee, M., 2014. ^{10}Be dating of boulders on moraines from the last glacial
544 period in the Nyainqentanglha mountains, Tibet. Science China (Earth Sciences), 57, 221–
545 231. Doi:10.1007/s11430-013-4794-z.
546 Dong, G., Xu, X., Zhou, W., Fu, Y., Zhang, L., Li, M., 2017. Cosmogenic ^{10}Be surface exposure
547 dating and glacier reconstruction for the last glacial maximum in the Quemuqu valley,
548 western Nyainqentanglha mountains, south Tibet. Journal of Quaternary Science, 32, 639-

652.

Dong, G., Zhou, W., Yi, C., Fu, Y., Zhang, L., Li, M., 2018. The timing and cause of glacial activity during the last glacial in central Tibet based on ^{10}Be surface exposure dating east of Mount Jaggang, the Xianza range. Quaternary Science Reviews, 186, 284-297.

Dortch, J.M., Owen, L.A., Caffee, M.W., 2013. Timing and climatic drivers for glaciation across semi-arid western HimalayaneTibetan orogen. Quaternary Science Reviews, 78, 188-208.

Doughty, A.M., Kaplan, M.R., Peltier, C., Barker, S., 2021. A maximum in global glacier extent during MIS 4. Quaternary Science Reviews, 261, 106948, ISSN 0277-3791, Doi:10.1016/j.quascirev.2021.106948.

Finkel, R.C., Owen, L.A., Barnard, P.L., Caffee, M.W., 2003. Beryllium-10 dating of Mount Everest moraines indicates a strong monsoon influence and glacial synchroneity throughout the Himalaya. Geology, 31, 561–564.

Gillespie, A., Molnar, P., 1995. Asynchronous maximum advances of mountain and continental glaciers. Review of Geophysics, 33, 311–364.

Ha, G., Wu, Z., He, L., Wang, S., 2018. Late Cenozoic Sedimentary Evolution of Pagri-Duoqing Co graben, Southern End of Yadong-Gulu Rift, Southern Tibet. Acta Geologica Sinica, 92, 972-987. doi: 10.1111/1755-6724.13586.

Hallet, B., Putkonen, J., 1994. Surface dating of dynamic landforms: young boulders on aging moraines. Science, 265, 937– 940.

Hedrick, K.A., Seong, Y.B., Owen, L.A., Caffee, M.C., Dietsch, C., 2011. Towards defining the transition in style and timing of Quaternary glaciation between the monsoon-influenced Greater Himalaya and the semi-arid Transhimalaya of Northern India. Quaternary International, 236, 21-33.

Herzschuh, U., 2006. Palaeo-moisture evolution in monsoonal Central Asia during the last 50,000 years. Quaternary Science Reviews, 25, 163–178.

574 Heyman, J., Stroeven, A.P., Harbor, J.M., Caffee, M.W., 2011. Too young or too old: evaluating
575 cosmogenic exposure dating based on an analysis of compiled boul-der exposure ages. Earth
576 and Planetary Science Letters, 302 (1–2), 71–80.
577 Heyman, J., 2014. Paleoglaciation of the Tibetan Plateau and surrounding mountains based on
578 exposure ages and ELA depression estimates. Quaternary Science Reviews, 91, 30-41,
579 doi:10.1016/j.quascirev.2014.03.018.
580 Iwata, S., Narama, C., Karma, 2002. Three Holocene and late Pleistocene glacial stages inferred
581 from moraines in the Lingshi and Thanza village areas, Bhutan. Quaternary International
582 97-98, 69–78.
583 Kohl, C.P., Nishiizumi, K., 1992. Chemical isolation of quartz for measurement of in situ-produced
584 cosmogenic nuclides. Geochimica et Cosmochimica Acta, 56, 3583–3587
585 Lal, D., 1991. Cosmic ray labeling of erosion surfaces: in situ nuclide production rates and erosion
586 models. Earth and Planetary Science Letters, 104, 429–439.
587 Lifton, N., Sato, T., Dunai, T.J., 2014. Scaling in situ cosmogenic nuclide production rates using
588 analytical approximations to atmospheric cosmic-ray fluxes. Earth and Planetary Science
589 Letters, 386, 149-160. doi: 10.1016/j.epsl.2013.10.052.
590 Lisiecki, L.E., Raymo, M.E., 2005. A Pliocene–Pleistocene stack of 57 globally dis-tributed benthic
591 δ18O records. Paleoceanography, 20 (1). Doi:10.1029/2004PA001071.
592 Liu, J., Yi, C., Li, Y., Bi, W., Zhang, Q., Hu, G., 2017. Glacial fluctuations around the Karola Pass,
593 eastern Lhagoi Kangri Range, since the Last Glacial Maximum. Journal of Quaternary
594 Science, 32, 516-527.
595 Mölg, T., Maussion, F., Scherer, D., 2013. Mid-latitude westerlies as a driver of glacier variability
596 in monsoonal High Asia. Nature Climate Change, 4, 68–73.
597 Owen, L.A., Finkel, R.C., Caffee, M.W., 2002. A note on the extent of glaciation in the
598 Himalaya during the global Last Glacial Maximum. Quaternary Science Reviews, 21, 147–

157.

Owen, L.A., Finkel, R.C., Barnard, P.L., Haizhou, M., Asahi, K., Caffee, M.W., Derbyshire, E., 2005. Climatic and topographic controls on the style and timing of Late Quaternary glaciation throughout Tibet and the Himalaya defined by 10 Be cosmogenic radionuclide surface exposure dating. Quaternary Science Reviews, 24 (12), 1391-1411.

Owen, L.A., Robinson, R., Benn, D.I. et al., 2009. Quaternary glaciation of Mount Everest. Quaternary Science Reviews, 28, 1412–1433.

Owen, L.A., Yi, C., Finkel, R.C., Davis, N., 2010. Quaternary glaciation of Gurla Mandata (Naimon'anyi). Quaternary Science Reviews, 29, 1817-1830.

Owen, L.A., Dortch, J.M., 2014. Nature and timing of Quaternary glaciation in the Himalayan-Tibetan orogen. Quaternary Science Reviews, 88, 14-54.

Peng, X., Chen, Y., Liu, G., Liu, B., Li, Y., Liu, Q., Han, Y., Yang, W., Cui, Z., 2019. Late Quaternary glaciations in the Cogarbu valley, Bhutanese Himalaya. Journal of Quaternary Science, 31, 40-50. Doi: 10.1002/jqs.3079.

Prell, W.L., Kutzbach, J.E., 1992. Sensitivity of the Indian monsoon to forcing parameters and implications for its evolution. Nature 360, 647–652.

Putkonen, J., Swanson, T., 2003. Accuracy of cosmogenic ages for moraines. Quaternary Research, 59, 255-261.

Qiu, J., 2008. China: The third pole. Nature 454, 393-396.

Ruddiman, W.F., Kutzbach, J.E., 1989. Forcing of Late Cenozoic northern hemisphere climate by plateau uplift in Southern Asia and the American West. Journal of Geophysical Research, 94, 18409–18427.

Schäfer, J.M., Tschudi, S., Zhao, Z., Wu, X., Ivy-Ochs, S., Wieler, R., Baur, H., Kubik, P.W., Schluchter, C., 2002. The limited influence of glaciations in Tibet on global climate over the past 170000 yr. Earth and Planetary Science Letters, 194, 287-297.

624 Shi, Y., 2002. Characteristics of late quaternary monsoonal glaciation on the Tibetan plateau and in
625 east Asia. Quaternary International, 97/98, 79-91.
626 Stone, J.O., 2000. Air pressure and cosmogenic isotope production. Journal of Geophysical
627 Research, 105, 23753–23759.
628 Wang, Y., Cheng, H., Edwards, R.L., Kong, X., Shao, X., Chen, S., Wu, J., Jiang, X., Wang, X.,
629 An, Z., 2008. Millennial- and orbital-scale changes in the East Asian monsoon over the past
630 224,000 years. Nature, 451, 1090–1093.
631 Wang, S., Chevalier, M.L., Pan, P., Bai, M., Li, K., Li, H., Wang, G., 2020. Quantification of the
632 late Quaternary activity of the Yadong rift, southern Tibet. Tectonophysics,
633 10.1016/j.tecto.2020.228545.
634 Yao, T., Thompson, L.G., Mosbrugger, V., Zhang, F., Ma, Y., Luo, T., Xu, B., et al., 2012. Third
635 Pole Environment (TPE), Environmental Development, 3, 52-64,
636 https://doi.org/10.1016/j.envdev.2012.04.002.
637 Yang, X., Li, L., Laba, Yang, X., Li, L., 2013. Study on the variation of lake area and its reasons
638 of Duoqing Lake in Tibet. Journal of Natural Research, 28, 625–634 (in Chinese with
639 English abstract).
640 Zech, R., Abramowski, U., Glaser, B., Sosin, P., Kubik, P.W., Zech, W., 2005. Late Quaternary
641 glacial and climate history of the Pamir Mountains derived from cosmogenic ^{10}Be exposure
642 ages. Quaternary Research, 64, 212–220.
643 Zech, R., Zech, M., Kubik, P.W., Kharki, K., Zech, W., 2009. Deglaciation and landscape history
644 around Annapurna, Nepal, based on ^{10}Be surface exposure dating. Quaternary Science
645 Reviews, 28, 1106-1118. Doi:10.1016/j.quascirev.2008.11.013.

Supplementary Material

Detailed description of the age compilation

1. Eastern transect: the Yadong-Gulu rift

In the southern part of the Yadong rift, in the Pagri basin, the two moraines we dated, Qudui and Jichu (#3 and #1 in Figs. 5, 6 and Table 2, respectively), are LGM and MIS-3, respectively, as discussed in the main text. Between Jichu and Qudui, Wang et al. (2020) obtained a LGM age for a small recessional moraine (?) located on the western slopes of the Chomo Lhari Range (moraine Duina, #2). Downstream from Duina (#2'), Ha et al. (2018) dated the smooth surfaces as MIS-6 using OSL dating, as explained in main text. Farther north in the central Yadong rift, on the northern slopes of the Bhutanese Himalaya, Peng et al. (2019) dated seven of the nine imbricated moraines from the Cogarbu Valley (#4), the largest of which (M5) is LGM. In the northern Yadong rift near the Karola pass, Owen et al. (2005) dated the most extensive moraine as LGM ('Karola', #5), similarly to Liu et al. (2017) on the western and eastern sides of the neighboring Nonn Kang Range (M4W and M4E, #6 and 7, respectively).

In the northern Yadong-Gulu rift, there are four studies from the SE slopes of the NQTL Range and one from its NW slopes. In the Quemuqu Valley of the Qiongmu Gangri Mountain (7048 m), located at the SW end of the NQTL Range, Dong et al. (2017) dated the inner Quemuqu moraine as LGM (#8). About 20 km to the north, Chevalier et al. (2011, 2020) dated two imbricated moraines near Yangbajing, the inner one being LGM and the outer one being MIS-4 ('Ybj', #9). On the northern slopes of the NQTL Range at Payuwang, Dong et al. (2014) dated two imbricated moraines, which oldest ages are both MIS-3 (#10 and 10'). At the northern end of the range, Owen et al. (2005) dated a small moraine in the 'Gulu south' valley as LGM as well as a hummocky moraine much farther downstream (on the opposite side of the Gulu basin) (#11), with a scattered and continuous age distribution, that we interpret as a degraded MIS-6 (hence the purple circle in Fig. 6) as inferred from eastern Tibet (Chevalier and Replumaz, 2019). In the valley just to the north,

671 Chevalier et al. (2011, 2020) determined a LGM age for the Gulu moraine (#12).

672 **2. Central N-S transect: the Dinggye-Xainza rift**

673 West of the Yadong-Gulu rift, two moraines have been dated in the Dinggye rift on the
674 eastern slopes of the Ama Drime massif (Chevalier et al., 2011). The most extensive moraine at
675 “Dinggye S” is MIS-3 (#13 in Figs. 5, 6 and Table 2) and the inner one is LGM. Ages from the
676 “Dinggye N” moraine (#14) continuously range from 20 to 195 ka (after rejecting one outlier at 320
677 ka) hence it belongs to MIS-6. In the Xainza rift to the north, Chevalier et al. (2011) dated five
678 moraines: the southernmost three are MIS-3 (moraines #15, 16 and 17, respectively), moraine #18 is
679 MIS-4, and moraine #19 is MIS-6. At the northern end of the Xainza Range, Dong et al. (2018)
680 dated seven imbricated moraines from Mt. Jaggang: three LGM, three MIS-3 (not shown in Fig. 5
681 because not the largest), and one MIS-4 (#20). This site is the only one where both MIS-3 and MIS-
682 4 advances have been documented so far, suggesting a MIS-4 glacial advance at least at some places
683 in Tibet (Doughty et al., 2021). Nevertheless, as said in the main text, further dating would be
684 necessary to advance on this topic, which is beyond the scope of this paper, as the two sites we
685 study here do not show MIS-4 ages.

686 **3. Western N-S transect: Kung Co rift**

687 The two moraines from yet the next rift to the west, the Kung Co rift, are MIS-3 (Cho Oyu,
688 #21 in Figs. 5, 6 and Table 2), and MIS-4 (Kung Co, #22) (Chevalier et al., 2011).

689

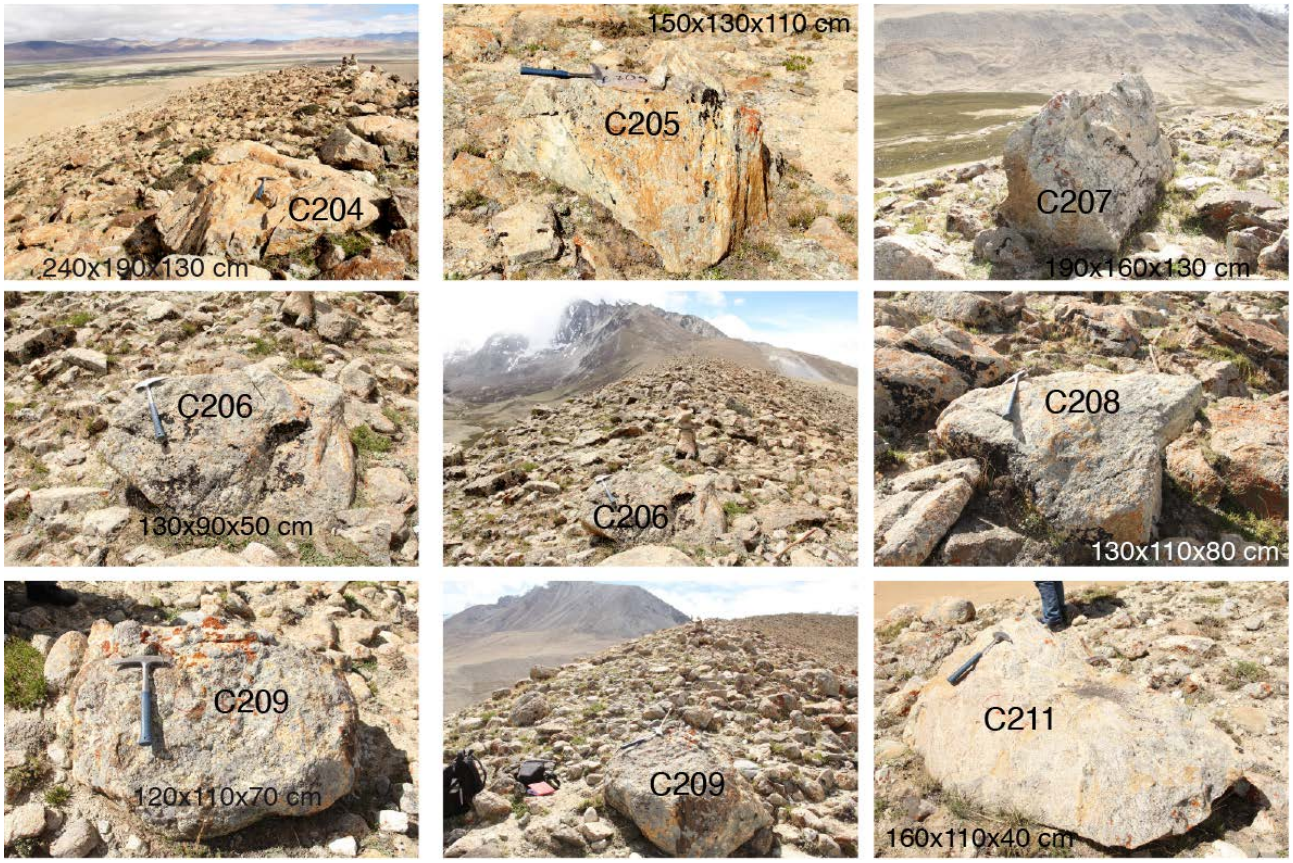

690

691 ***Figure S1**: Photos of boulders collected for ^{10}Be surface-exposure dating at the Qudui moraine site*

692 *with their approximate sizes.*

693

694 ***Figure S2**: Photos of boulders collected for ^{10}Be surface-exposure dating at the Jichu moraine site*

695 *with their approximate sizes.*

696

697 ***Table S1:** Application of Peirce's criterion on the age compilation.*

698

699 ***Table S2:** Age compilation of the most extensive moraines from the broad Yadong region.*